Accepted Manuscript

Title: Vein graphite-based counter electrodes for dye-sensitized solar cells

Authors: E.N. Jayaweera, G.R.A. Kumara, H.M.G.T.A. Pitawala, R.M.G. Rajapakse, N. Gunawardhana, H.M.N. Bandara, A. Senarathne, C.S.K. Ranasinghe, Hsin-Hui Huang, M. Yoshimura

Vein graphite-based counter electrodes for dye-sensitized solar cells

E. N. Jayaweera[a], G. R. A. Kumara[a,*], H. M. G. T. A. Pitawala[b], R. M. G. Rajapakse[a], N. Gunawardhana[c], H. M. N. Bandara[a], A. Senarathne[b], C. S. K. Ranasinghe[a], Hsin-Hui Huang[d], M. Yoshimura[d]
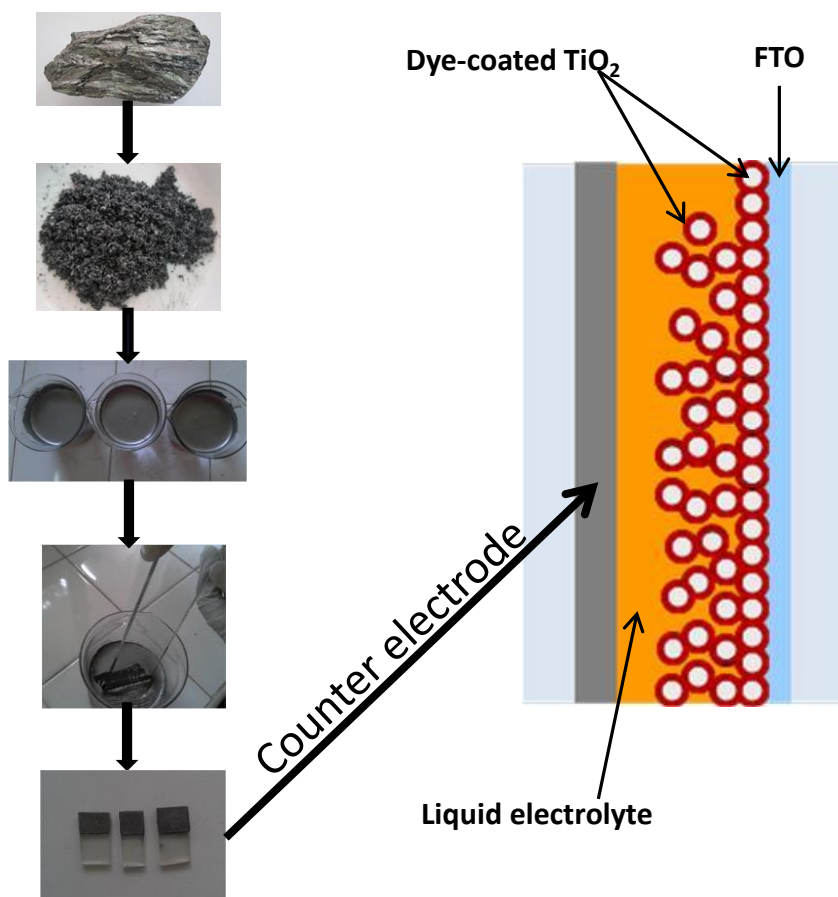
[a] Department of Chemistry, University of Peradeniya, Peradeniya, Sri Lanka
[b] Department of Geology, University of Peradeniya, Peradeniya, Sri Lanka
[c] International Research Centre, University of Peradeniya, Peradeniya, Sri Lanka
[d] Graduate School of Engineering, Toyota Technological Institute, Nagoya, Japan

Graphical abstract

Highlights

- Purified Sri Lankan vein graphite has been used as counter electrode material in dye-sensitized solar cells (DSCs).
- We devised a novel technology for graphite enrichment in which the ball-milled Sri Lankan graphite (BMG) was floated in water.
- Ball-milled floated graphite (BMFG) was separated and both BMG and BMFG were extensively characterized for the first time.
- It has been found that the floating technology has increased the defect sites that act as catalytic sites for I_3^- reduction.
- It has been found that BMFG is a better counter electrode material than BMG for applications in DSCs.

ABSTRACT

This paper describes the use of ball-milled vein graphite and ball-milled floated graphite counter electrode (CE) materials in dye-sensitized solar cells. The vein graphite used was ball milled, sieved and fraction of

particle sizes in the 45–63 µm was used (BMG). Another fraction in the same size range was floated in water to get ball-milled floated graphite (BMFG). Both samples were extensively characterized by electrochemical techniques, Raman spectroscopy and by Total Carbon Analysis. The performance of dye-sensitized solar cells (DSCs) prepared using these CEs were optimized for their adhesion, sintering temperature and thickness. Best performances were obtained for the DSC with CE prepared using graphite:morphol mass ratio of 5:3, sintering temperature of 350 ˚C and the thickness of 250 µm. Most of the impurities in ball-milled graphite can be removed by the floating technique and the DSC fabricated with ball-milled floated graphite based CE gives 24% better performance than that constructed using just ball-milled graphite based CE. The best conversion efficiency observed is 6.47%. Though this is less than that obtained using Pt CE, it is still very useful in practical applications as per cost considerations.

Keywords: dye-sensitized solar cell; counter electrode; vein graphite; flotation

*Corresponding author

G. R. A. Kumara, Department of Chemistry, University of Peradeniya, Peradeniya, Sri Lanka

E-mail: grakumara2000@yahoo.com

1. INTRODUCTION

Dye-sensitized solar cells (DSCs) have received a great deal of interest due to their proven potential for future photovoltaic (PV) applications. In terms of cost, ease of fabrication and decorative nature, DSCs outrun other emerging and conventional PV technologies. The major breakthrough in the field of DSCs came with the report of O'Regan and Grätzel published in 1991 [1]. A mesoporous, interconnected nanoparticulate TiO_2 film deposited on F-doped SnO_2 conducting layer on glass (FTO) and a novel Ru-based dye together with liquid electrolyte containing I^-/I_3^- redox couple in acetonitrile and a lightly platinized FTO counter electrode were the components utilized in this DSC. The device had an impressive power conversion efficiency, η, of 7.1% – 7.9% in AM 1.5 illumination and 12% in the diffuse daylight together with over 80% IPCE. This very device correspond to a remarkable increase in the efficiency compared to the early reported DSCs mainly owing to the large surface area provided by the mesoporous nature of the TiO_2 film for monolayer dye coverage. The porous nature could increase the effective surface area for the dye adsorption by c.a.780-fold compared with that of the flat electrode used earlier [1].

Unlike in other conventional PV technologies, in DSCs, the function of charge generation is being separated from the charge transportation. A mesoporous interconnected semiconductor nanoparticulate network has been employed to achieve efficient charge separation from the excited dye molecules anchored onto the semiconductor particle surfaces

The counter electrode (CE) used in DSCs should fulfil certain requirements. It should be an excellent catalyst for the regeneration of the reduced species by reducing the oxidized species present in the electrolyte. DSCs with the configuration $FTO/TiO_2/N749$ Dye/I^--I_3^- in acetonitrile electrolyte/Pt-FTO have produced maximum efficiencies over 11% when recombination of injected electrons and dye aggregations are suppressed by using suitable additives [2]. Charge transfer resistances that are less than 1 Ω cm^2 had been achieved for Pt-CEs [3]. Long term stability of the CE material and good electrical conductivity are other parameters that determine the choice of materials for the CE of DSCs. The material requirement has been much lowered by lightly platinizing FTO plates for use in DSCs. Nonetheless, the high cost of Pt CEs has made them unfeasible for large scale applications [4]. Hence, this has encouraged research in search of low-cost alternatives to Pt-based CEs. In such alternatives, carbon materials including, carbon black [5], carbon nanotubes [6-8], activated carbon [9], graphite [10,11], graphene [12,13], and conducting polymers [14,15] have been tested.

Of these alternative CE materials, graphite, a naturally occurring allotrope of carbon, is considered a potential candidate owing to its high abundance, low-cost, favourable electrical, thermal and catalytic properties. The different structural regions of graphite known as basal planes and edge planes show different electro-catalytic activities [16]. These edge planes act as superior catalytic sites compared with the basal planes for the reduction of I_3^- [11].

In this study, Sri Lankan vein graphite was used to fabricate low-cost CEs for DSCs. Here, a simple purification method has also been employed to significantly improve the performance of the relevant CEs. Though the origin of the vein graphite found in Sri Lanka is still under debate, it is suggested that the magmatic origin is preferred over granulite facies metamorphism [17-19]. Sri Lankan vein graphite is well-known for its high purity and crystallinity. Nevertheless, the existence of gangue minerals such as pyrite, calcopyrite, calcite etc. either physically attached or intercalated into graphite has been reported [18]. Physical and chemical purification processes have, therefore, been employed to remove the undesirable gangue minerals [20,21]. Since, impurities occurring in graphite could hamper the performance of graphite-based counter electrodes, a simple floatation method was used in this study to improve the purity of graphite samples. Separation of hydrophobic graphite particles by an air bubble-assisted floatation method could enhance the purity of the graphite. In this publication, we reveal the development of CEs from Sri Lankan vein graphite and their applications in liquid electrolyte-based DSCs. For comparison, usual FTO-Pt based DSCs were also fabricated and the performances are compared.

2. EXPERIMENTAL METHODS

2.1. Preparation of TiO₂ colloidal solution

First, titanium tetraisopropoxide (20.0 ml) (Kanto Chemicals, Japan 97%) and acetic acid (2.5 ml) (Wako Chemicals, Japan, 99.7%) were mixed with ethanol (25.0 ml) (Hayman, England, 99.9%) and steam was passed through the solution for 2 min. Rapid hydrolysis of titanium tetraisopropoxide and the expulsion of ethanol by steaming then produced a transparent solid mass consisting of TiO_2 nanoparticles. This solid mass was ground with 50.0 ml of water in a motor and subsequently autoclaved at 150 °C for 3 hours.
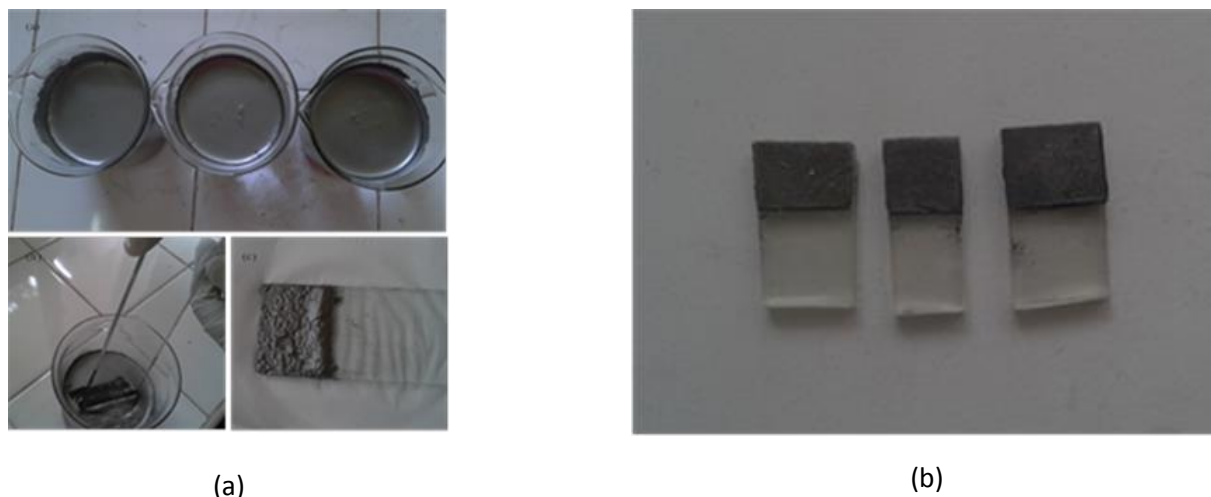
2.2. Preparation of dye-coated TiO₂ working electrode

TiO_2 suspension for spray pyrolysis was prepared by mixing titanium dioxide colloidal solution (20.0 ml), acetic acid (5.5 ml) and Triton X-100 (5 drops) (Sigma, USA, 99.5%) and it was further diluted by adding ethanol (20.0 ml). The cleaned FTO glass plates were kept on a hot plate heated at 150 °C and the TiO_2 suspension was sprayed onto the FTO glass. These plates were sintered at 500 °C for 30 min, in air, and allowed to gradually cool down to about 80 °C. The warm plates were then placed and kept soaked overnight in a 0.3×10^{-3} M solution of di-tetrabutylammonium-cis-bis(isothiocyanato)bis(2,2'-bipyridyl-4,4'-dicarboxylate)ruthenium(II) (N719) dye in a 1:1 solvent mixture of acetonitrile and tertiary-butyl alcohol. They were subsequently taken out of the dye solution, rinsed with acetonitrile and used as working electrodes of DSCs. **Purification of ball-milled vein graphite using floatation method**

Graphite samples were collected from Bogala mine, Sri Lanka, and ball-milled, for 20 min, using a Pritsch Pulverisette 6 ball-milling instrument. The resulted powder was sieved to separate particles in the size range 45–63 μm. Then, ball-milled and sieved graphite powder was added to de-ionized water and subjected to continuous stirring. The graphite layer which was subsequently formed at the surface of the water was removed using glass slides and dried in an air flow. Fig. 1(a) illustrates, in pictorial manner, the steps involved in obtaining the floated graphite layer. We denote this as-collected graphite as BMFG and ball milled-graphite as BMG.

2.3. Preparation of graphite counter electrodes and cyclic voltammetric (CV) characterization

A mixture of BMFG, morphol (Phenanthrene-3,4-diol) (Molbase, China, 98%) and de-ionized water (9.5 ml) was stirred overnight and was heated at 80 °C to evaporate the excess water in the paste. Graphite films with surface area of 1 cm^2 were then deposited on the FTO plates using the doctor-blade technique. First the composition of the graphite paste and the sintering temperature of counter electrodes were optimized using J-V characteristics. In this regard thickness of the graphite films were maintained at 330 µm. Then the thickness of the graphite films was also varied in order to identify the optimum thickness. The BMFG-deposited FTO plates were then sintered for 30 min at 350 °C. Photograph of the CEs prepared is shown in Fig. 1 (b). In order to study and compare the effect of purification of the graphite on the performance of DSCs, counter electrodes were prepared using the untreated graphite (BMG) also.

(a)

(b)

Fig. 1. (a) Floated graphite layer formed at the surface of water, removal of the floated graphite layer using a glass slide and as-collected graphite (BMFG) on glass and (b) graphite counter electrodes prepared using doctor-blade method.

The CV studies of counter electrodes based on BMFG, BMG and Pt/Cr-mirror type were carried out in an acetonitrile electrolyte containing 10 mM LiI, 1 mM I$_2$ and 0.1 M NaClO$_4$ at a scan rate of 50 mV s^{-1}. The reference and the counter electrode used were Ag/AgCl electrode and Pt-gauze electrode, respectively.

2.3. Fabrication of DSCs

The dye-coated TiO$_2$ working electrodes were sandwiched with graphite-CEs and the space between two electrodes was filled with an electrolyte containing 0.1 M LiI, 0.05 M I$_2$, 0.6 M dimethylpropylimidazolium iodide and tert-butylpyridine in acetonitrile. J-V characteristics for the DSCs were recorded using a PECcell-L01 solar simulator coupled to a Keithley (2400 model) multimeter, under AM 1.5 illumination. Here, a mask was used to make the active area of the cells as 0.25 cm^2.

2.3. Other Characterizations

Raman spectroscopy measurements were taken using a Renishaw InVia Reflex Raman microscopy system with a 532 nm laser. Total carbon analyses of graphite samples were performed by carbon/sulfur analyzer (Eltra CS-2000) at Activation Laboratories Ltd., Ontario, Canada.

3. RESULTS AND DISCUSSION

3.1. Graphite Concentration

The carbon content determined which are given in Table 1 reveal a notable enhancement in the purity of graphite collected by floatation method (BMFG). The total carbon percentage of the BMFG (in the particle size range of 45 – 63 µm) increased from 91.9% to 98.0% compared to the original BMG sample. This simple

floatation method resulted in an appreciable increase in the purity of graphite samples, and the use of such high quality graphite in counter electrodes gives better DSC performance as will be revealed later.
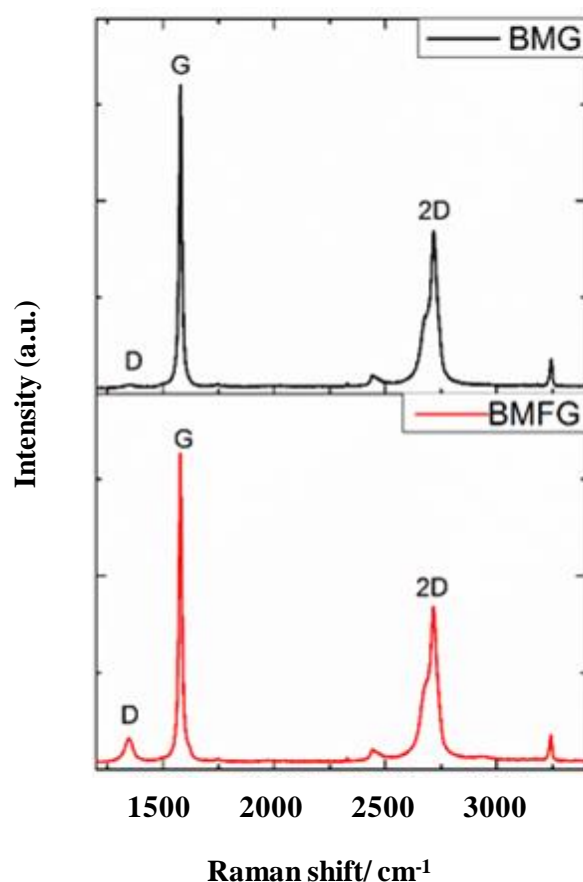
Table 1. Carbon content of the graphite samples as determined by total carbon analysis.

Carbon Content as Weight%	High	Moderate	Low
BMG	95.9	92.9	91.9
BMFG	98.0	97.3	98.0

3.2. Raman Spectroscopic Characterization

The atomic arrangement in graphite is known to result in a heterogeneous electrochemical behavior. The stacked arrangements of 2-dimensional graphite layers give rise to two types of graphitc planes, namely; basal planes and edge planes [16]. These two planes exhibit distinctive electrochemical properties owing to their inherent electron transport properties. In this regard, edge planes show faster electron tranfer kinetics and consequently higher catalytic activity compared to that of basal planes. In the context of DSCs, edge planes of graphite in counter electrode (CE) serve as catalytic sites for I_3^- reduction. Thus, having a higher degree of edge planes in the CE would be advantageous.

Raman spectroscopic studies provide valuable information on the degree of disorder and defects present in a given graphite sample. In general, peaks appearing in Raman spectra at 1355 cm^{-1} and 1580 cm^{-1} are assigned to D band and G band, respectively, where D band corresponds to the degree of disorder in graphite and G band corresponds to the in-plane optical mode [16]. Hence, the intensity of D band depends on the particle size and defects present in graphite. The Raman spectra obtained for BMG and BMFG are shown in Fig. 2. For both BMG and BMFG samples, the two peaks corresponding to D and G bands appear at 1347 cm^{-1} and 1579 cm^{-1}, respectively. Intriguingly, the intensity of the peak corresponding to D band has increased for BMFG. Accordingly, the ratio of I_D/I_G, for BMFG and BMG is calculated to be 0.10 and 0.03, respectively. Therefore, it can be assumed that the floatation method has resulted in smaller crystallite sizes and consequently larger number of edge sites compared to the BMG samples. Since the presence of disorder and defects is desirable to ensure efficient reduction of I_3^-, higher number of edges present in these BMFG materials, as inferred from the Raman spectroscopic studies, is obviously advantageous for the performance of graphite CEs. These results suggest that BMFG is better than BMG for application as CEs in DSCs.
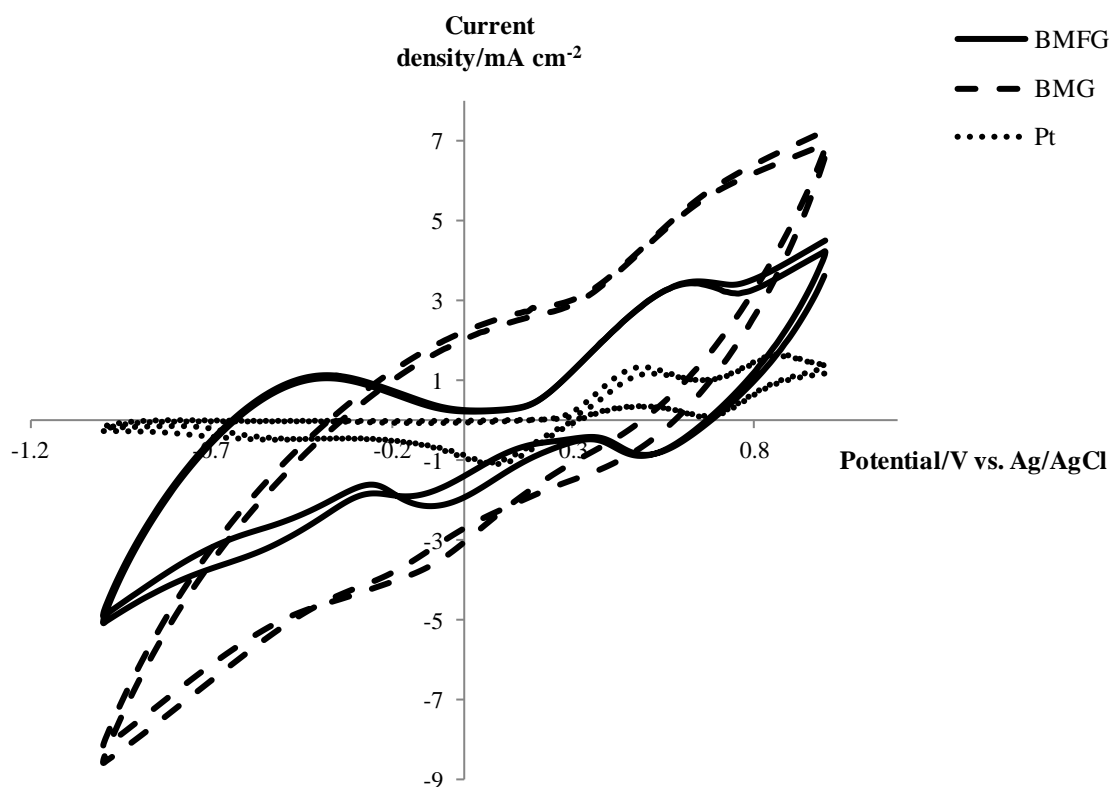
Fig. 2. Raman spectra of the BMG (upper) and BMFG (lower) samples. The D band appears in BMFG sample due to the edge effects.

3.3. Cyclic voltammetric studies

The cyclic voltammograms obtained for the redox reaction of I^-/I_3^- with two graphite CEs and Pt CE are shown in Figure 3. The cathodic and anodic peaks observed in the cyclic voltammogram can be assigned to the reduction of I_3^- and the oxidation of I^-, respectively.

According to Fig. 3, the current density corresponding to the I_3^- reduction peak varies as BMG > BMFG > Pt. In general, high current densities of the cathodic peak dictate the high catalytic activity towards I_3^- reduction. In this regard, the graphite electrodes show higher catalytic activity than Pt counterpart. This could be possible as the thickness of the graphite layers are several orders of magnitude higher compared to that of Pt CE. Further, different current densities are observed for BMFG and BMG, which have similar graphite layer thickness. The observed increase in the peak current density for BMG electrode compared to that of BMFG electrode can thus inevitably be a consequence of impurities present. Furthermore, broadening of the respective voltammogram and the shift observed in the peaks confirm the building up of a high double layer capacitance for both graphite electrodes. The porous nature of these electrodes could have facilitated the building up of double layer capacitance, which is obviously disadvantageous. Moreover, broadening of the voltammogram is higher for BMG electrode compared to that of BMFG electrode, and this can also be due to the presence of impurities. Therefore, it can be concluded that the purification employed in this study is indeed effective in removing impurities which could otherwise hinder the performance of the CE.

Fig. 3. Cyclic voltamograms of electrodes based on BMFG, BMG and Pt/Cr-mirror type, in 10 mM LiI, 1 mM I_2, 0.10 M $NaClO_4$ in an acetonitrile electrolyte, at 50 mV s-1 obtained using Ag/AgCl reference electrode and Pt-gauze counter electrode.

3.4. Optimization of DSC performance: Effect of binder on counter electrode characteristics

This is the first time report of the morphol as a binder for graphite. Optimization of the counter electrode involves optimizing the graphite to binder ratio in the graphite paste, sintering temperature and the thickness of the graphite layer. In this context, first, the optimum composition of the graphite paste was determined by varying the amount of morphol added to 0.100 g of BMFG. Here, BMFG CEs having a graphite layer thickness of 330 μm were prepared and sintered at 350 °C. The photovoltaic parameters of the DSCs constructed are summarized in Table 2. As evident from the photovoltaic performances, the optimum composition of morphol in the paste corresponds to a graphite:binder (w/w) ratio of 5:3. At very low morphol concentrations, overall performance of the respective DSC seems to get severely hindered. This is mainly attributed to the poor adhesion of graphite layer to the FTO substrate. Peeling off of the graphite layer was observed for very low morphol concentrations. As the weight of the morphol increases from 0.020 g to 0.060 g, η increases mainly owing to the increase in the FF and J_{SC}. Consequently, an efficiency of 5.43% is obtained for the DSC, where the CE corresponds to graphite:morphol ratio of 5:3. Then, on further increasing morphol, FF and J_{SC} tend to decrease. The attenuation observed in FF and J_{SC} reveals that dye regeneration kinetics must have got hindered due to the sluggish reduction of I_3^- at the CE. This further reflects that the high morphol content gives rise to poor electrical conductivity of the graphite film, which in turn results in slower electron transfer rates to the I_3^- ions at the CE. Moreover, it can be observed that, at moderate morphol contents, the V_{OC} of DSCs is less sensitive to the composition of the CE. However, at extreme conditions, a considerable decrease in the V_{OC} is also observed. Therefore, these results suggest that, at very low morphol concentrations, poor adhesion of graphite layer to the FTO results in low electrical

7

conductivities of the CE. On the other hand, high concentrations of morphol give rise to sluggish electron transfer kinetics, owing to the poor electrical connection between graphite particles.

Table 2. Photovoltaic parameters of DSCs employing BMFG-based CE[a] prepared with different amounts of morphol.

Mass of morphol added to 0.10 g of graphite/g	Graphite:Morphol mass ratio	J_{SC}/mAcm^{-2}	V_{OC} /V	FF	η/%
0.02	5:1	8.92	0.670	0.22	1.32
0.04	5:2	11.64	0.706	0.55	4.55
0.06	5:3	13.44	0.700	0.58	5.43
0.08	5:4	11.51	0.708	0.44	3.60
0.10	1:1	10.12	0.635	0.36	2.31

[a] Here, CEs having a graphite layer thickness of 330 μm were sintered at 350 °C

3.5. Optimization of DSC Performance: Effect of sintering temperature of the counter electrode

J-V characteristic of the DSC, where CEs having a graphite layer thickness of 330 μm, but sintered at different temperatures, ranging from 250 °C to 400 °C, are summarized in Table 3. Interestingly, the corresponding DSCs prepared using CEs which were sintered at 300 °C and 350 °C show comparable efficiencies. Nevertheless, sintering temperature of 350 °C gives the highest efficiency of 5.67%, with a J_{SC} of 13.47 mA cm^{-2}, V_{OC} of 0.704 V and a FF of 0.54. Increasing the sintering temperature to 400 °C attenuates the performance of DSCs. In the optimization of the binder concentration, counter electrodes were sintered at 350 °C

In counter electrodes prepared at very low sintering temperatures binder is present in larger amounts and therefore the resistance of the graphite counter electrode is very high and thus the efficiency of the DCS is very low. At the moderate temperatures of 350 °C binder is burnt to a certain extent which is sufficient to provide good adhesion between graphite particles and between graphite layer and FTO, while giving low resistance values. As the sintering temperature increases, binder burns completely resulting in poorly adhered graphite films thus giving poor performance.

Therefore, it can be inferred that the performance of graphite CEs is determined by the compromise between the electrical conductivity and the degree of adhesion of graphite layer to the FTO substrate.

Table 3. Photovoltaic parameters of DSCs employing graphite CEs sintered at different temperatures.

Temperature/ °C	J_{SC} /mA cm^{-2}	V_{OC} /V	FF	η/%
250	10.24	0.653	0. 34	2.29
300	13.21	0.717	0.54	5.10
350	13.47	0.704	0.60	5. 67
400	12.82	0.700	0.49	4.43

[a] Here, CEs having a graphite layer thickness of 330 μm were prepared using the paste with the graphite:binder (w/w) ratio of 5:3

3.6. Optimization of DSC Performance: Effect of thickness of the counter electrode

Finally, the thickness of the graphite CE was optimized. Here, all the CEs were prepared using the optimized paste and were sintered at 350 °C. The *J-V* characteristics obtained to investigate the effect of graphite layer thickness on the performance of DSCs are shown in Table 4. The highest efficiency of 6.47% is obtained for the DSC employing a CE with a graphite layer thickness of 250 μm. For a lower thickness of graphite layer than this, the corresponding J_{SC}, V_{OC} and consequently the efficiency seem to decrease. The low J_{SC} obtained for the graphite layer thickness of 160 μm can be ascribed to its lower catalytic activity. Apparently, the amount of graphite included in 160 μm thick layer is insufficient to render the required catalytic activity for the efficient reduction of I_3^- ions. On the contrary, as the graphite layer thickness is increased further, the efficiency of DSCs tends to decrease. Although, it is expected to improve the catalytic activity by increasing the thickness of the graphite layer, the results suggest that the catalytic activity alone cannot improve the performance of the CE. Resistance of the graphite layer and the thickness of the DSC are decisive in this regard. This is obviously confirmed by the decrease observed in J_{SC} and FF. As the thickness of the graphite layer increases from 250 μm to 550 μm, J_{SC} drops from 13.95 mA cm^{-2} to 9.93 mA cm^{-2} and FF decreases from 0.643 to 0.480.
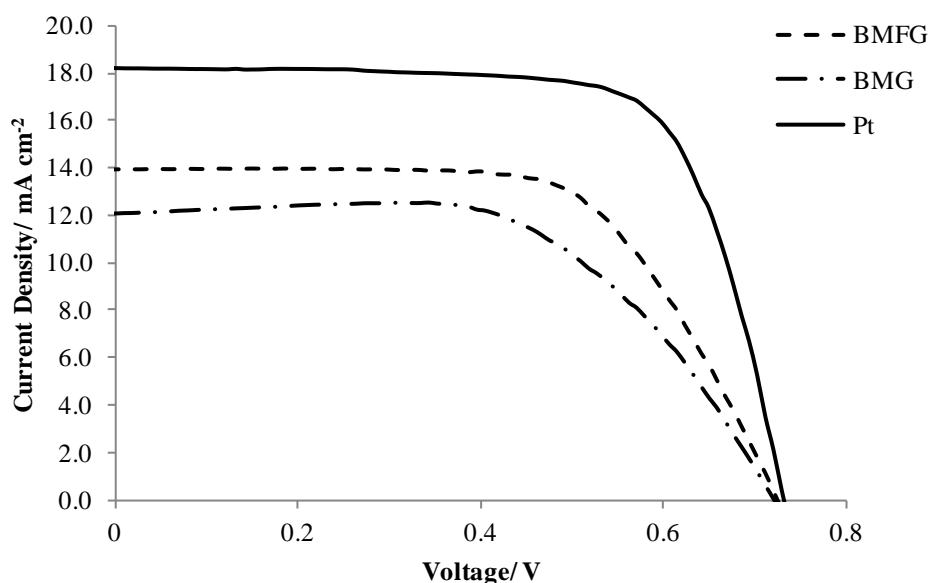
Table 4. Photovoltaic parameters of DSCs employing CEs[a] with different thicknesses of the graphite layer

Thickness/μm	J_{SC} /mA cm^{-2}	V_{OC} /V	FF	η/%
160	12.94	0.714	0.64	5.94
250	13.89	0.725	0.64	6.47
330	13.57	0.716	0.59	5. 78
460	12.37	0.701	0.53	4.56
550	9.93	0.703	0.48	3.35

[a] Here, CEs were prepared using the paste with the graphite:binder (w/w) ratio of 5:3 and were sintered at 350 °C

3.7. Optimization of DSC Performance: Effect of purity of graphite used in the counter electrode

In order to examine the effect of purification on the performance of the graphite CEs, J-V characteristics were obtained for the DSCs employing BMG-based CEs. For comparison purposes, J-V characteristics of DSCs employing a Pt CE were also recorded. The J-V characteristics of DSCs employing BMG-based CE, BMFG-based CE and Pt counter electrodes are shown in Fig. 4. Table 5 summarizes the corresponding photovoltaic parameters. Though both the graphite CEs show comparable V_{OC} values, a significant improvement in J_{SC} is observed for the BMFG-based CE compared to that of the BMG counterpart. Further, low FF observed for BMG-based CE reveals that the impurities present hinder the performance significantly. Purification of graphite thus results in increasing the efficiency of the DSC by a factor of 24%. Therefore, it can be proved that the simple purification process employed in this study is indeed effective. Obviously, Pt CE shows the highest efficiency of all.

Fig. 4. J-V characteristics of DSCs employing CEs prepared using BMG, BMFG and Pt CEs.

Table 5. Photovoltaic parameters of DSCs employing CEs with different compositions

Counter electrode	J_{SC} /mA cm^{-2}	V_{OC} /V	FF	$\eta(\%)$
FTO/BMFG	13.89	0.725	0.64	6.47
FTO/BMG	12.04	0.726	0.60	5.21
FTO/Pt-Cr	18.18	0.732	0.72	9.60

[a] Here, BMG and BMFG CEs having graphite film thicknesses of 250 μm were prepared using the paste with the graphite:binder (w/w) ratio of 5:3 and were sintered at 350 °C

4. CONCLUSIONS

Practical applications of dye-sensitized solar cells have been hampered due to several reasons and the cost of platinum counter electrode is one such factor. Replacement of platinum by low-cost materials is state-of-the-art research and carbon based materials are best choices. We developed a simple technique for graphite enrichment in which we have used a simple floating technique to remove impurities present in ball-milled Sri Lankan vein graphite. The use of ball-milled and floated Sri Lankan vein graphite as counter electrode material in dye-sensitized solar cells give the best efficiency of 6.47%. Though this efficiency is less than that obtained with platinum based dye-sensitized solar cells, as per cost considerations lower efficiency with a cheap DSC may be more viable for practical applications than expensive DSC with higher efficiency.

REFERENCES

[1] B. O'Regan, M. Grätzel, A low cost, high efficiency solar cell based on dye- sensitized colloidal TiO$_2$ films, Nature 353 (1991) 737-738.

[2] Y. Chiba, A. Islam, Y. Watanabe, R. Komiya, N. Koide, L. Han, Dye-Sensitized Solar Cells with Conversion Efficiency of 11.1%, Jpn. J. Appl. Phys. 45 (2006) L638–L640.

[3]   A. Hagfeldt, G. Boschloo, L. Sun, L. Kloo, H. Pattersson, Dye-sensitized solar cells. Chem. Rev. 110 (2010) 6595-6663.

[4]   J.M. Kroon, N.J. Bakker, H.J.P. Smit, P. Liska, K.R. Thambi, P. Wang, S.M. Zakeeruddin, M. Grätzel, A. Hinsch, S. Hore, U. Wurfel, Nanocrystalline dye-sensitized solar cells having maximum performance, Prog. Photovlot. Res. Appl. 15 (2007) 1–18.

[5]   T.N. Murakami, S. Ito, Q. Wang, M.K. Nazeeruddin, T. Bessho, I. Cesar, P. Liska, R. Humphry-Baker, P. Comte, P. Péchy, M. Grätzel, Highly efficient dye-sensitized solar cells based on carbon black counter electrodes, J. Electrochem. Soc. 153 (2006) 2255–2261.

[6]   K. Suzuki, M. Yamaguchi, M. Kumagai, S. Yanagida, Application of Carbon Nanotubes to Counter Electrodes of Dye-sensitized Solar Cells, Chem. Lett. 32 (2003) 28–29.

[7]   W.J. Lee, E. Ramasamy, D.Y. Lee, J.S. Song Efficient dye-sensitized solar cells with catalytic multiwall carbon nanotube counter electrodes, Appl. Mater. Inter. 1 (2009) 1145–1149.

[8]   H. Zhu, H. Zeng, V. Subramanian, C. Masarapu, K.H. Hung, B. Wei, Anthocyanin-sensitized solar cells using carbon nanotube films as counter electrodes, Nanotechnology 19 (2008) 465204–465205.

[9]   S.H. Park, B.K. Kim, W.J. Lee, Electrospun activated carbon nanofibers with hollow core/highly mesoporous shell structure as counter electrodes for dye-sensitized solar cells. J. Power Sources 239 (2013) 122–127.

[10] Y.S. Wei, Q.Q. Jin, T.Z. Ren, Expanded graphite/pencil-lead as counter electrode for dye-sensitized solar cells, Solid-State Electronics 63 (2011) 76-82.

[11] G. Veerappan, K. Bojan, S.W. Rhee, Sub-micrometer-sized graphite as a conducting and catalytic counter electrode for dye-sensitized solar cells, ACS Appl. Mater. Interfaces 3 (2011) 857–862.

[12] J.D. Roy-Mayhew, D.J. Bozym, C. Punckt, I.A. Aksay, Functionalized graphene as a catalytic counter electrode in dye-sensitized solar cells, ACS Nano 4 (2010) 6203-6211.

[13] L. Kavan, J.H. Yum, M. Grätzel, Optically transparent cathode for dye-sensitized solar cells based on graphene nanoplatelets, Acs Nano 5 (2010) 165–172.

[14] Y. Saito, T. Kitamura, Y. Wada, S. Yanagida, Application of Poly (3, 4-ethylenedioxythiophene) to Counter Electrode in Dye-Sensitized Solar Cells, Chem. Lett. 31 (2002) 1060–1061.

[15] J. Xia, N. Masaki, K. Jiang, S. Yanagida, The influence of doping ions on poly (3, 4-ethylenedioxythiophene) as a counter electrode of a dye-sensitized solar cell, J. Mater. Chem. 17 (2007) 2845–2850.

[16] C.E. Banks, T.J. Davies, G.G. Wildgoose, R.G. Compton, Electrocatalysis at graphite and carbon nanotube modified electrodes: edge-plane sites and tube ends are the reactive sites, Chem. Commun. 7 (2005) 829–841.

[17] F.J. Luque del Villar, J.D. Pasteris, B. Wopenka, M. Rodas, J.F. Fernández Barrenchea, Natural fluid-deposited graphite: mineralogical characteristics and mechanisms of formation, Am. J. Sci. 298 (1998) 471-498.

[18] P. Touzain, N. Balasooriya, K. Bandaranayake, C. Descolas-Gros, Vein graphite from the Bogala and Kahatagaha–Kolongaha mines, Sri Lanka: a possible origin, The Can. Mineral. 48 (2010) 1373-1384.

[19] M.B. Katz, Graphite deposits of Sri Lanka: a consequence of granulite facies metamorphism, Mineral. Deposita 22 (1987) 18-25.

[20] K. Zaghib, X. Song, A. Guerfi, R. Rioux, K. Kinoshita, Purification process of natural graphite as anode for Li-ion batteries: chemical versus thermal, J. Power Sources, 119 (2003) 8-15.

[21] J.L. Shui, J. Zhang, C.X. Ding, X. Yang, C.H. Chen, Hydrothermal modification of natural graphite as an anode material for lithium secondary batteries, Materials Science and Engineering B 128 (2006) 11-15.

Figure Caption

Figr-1

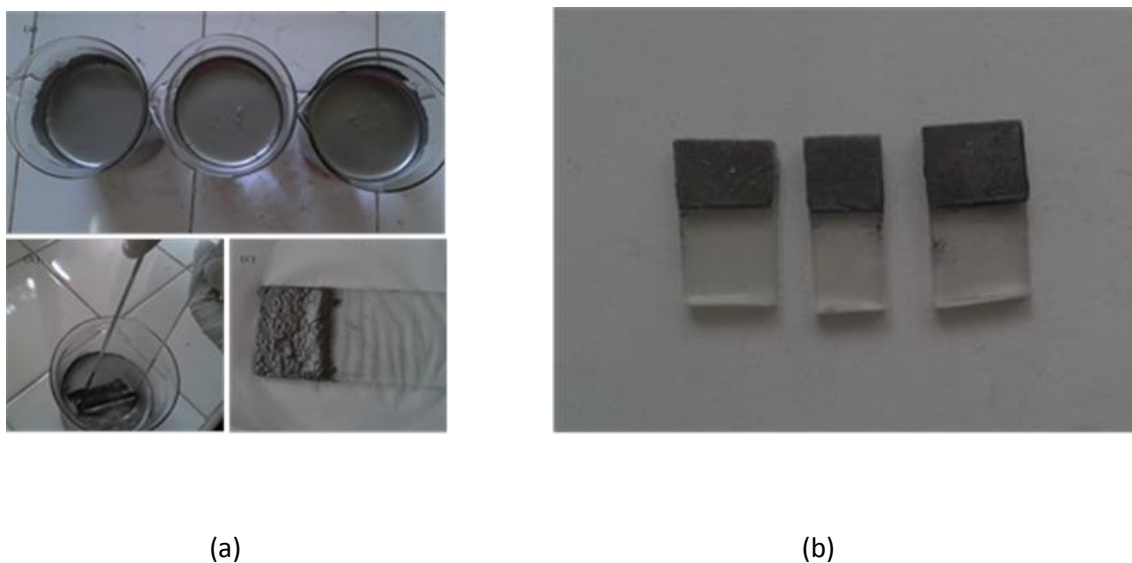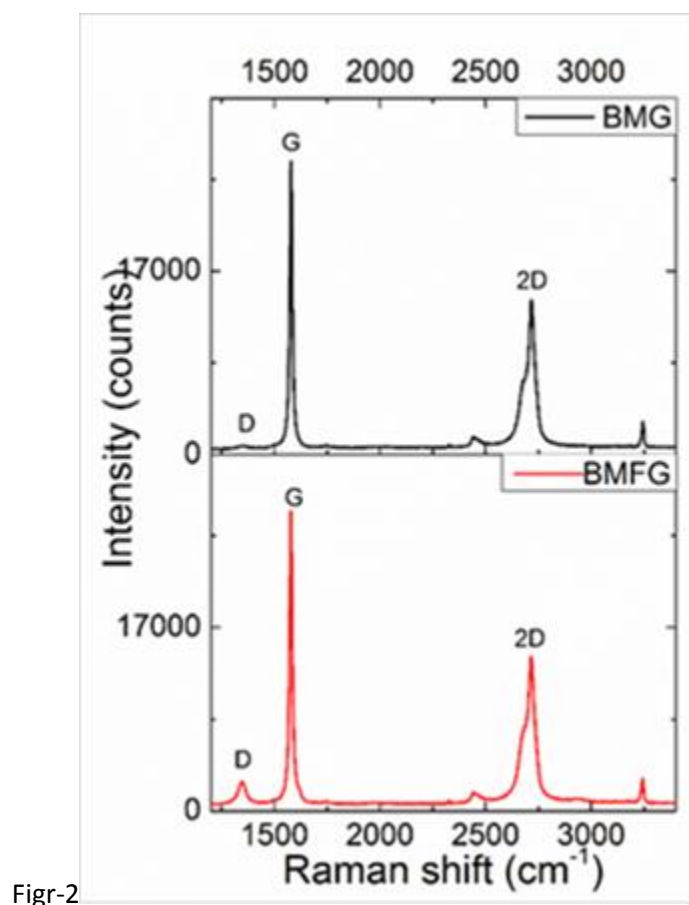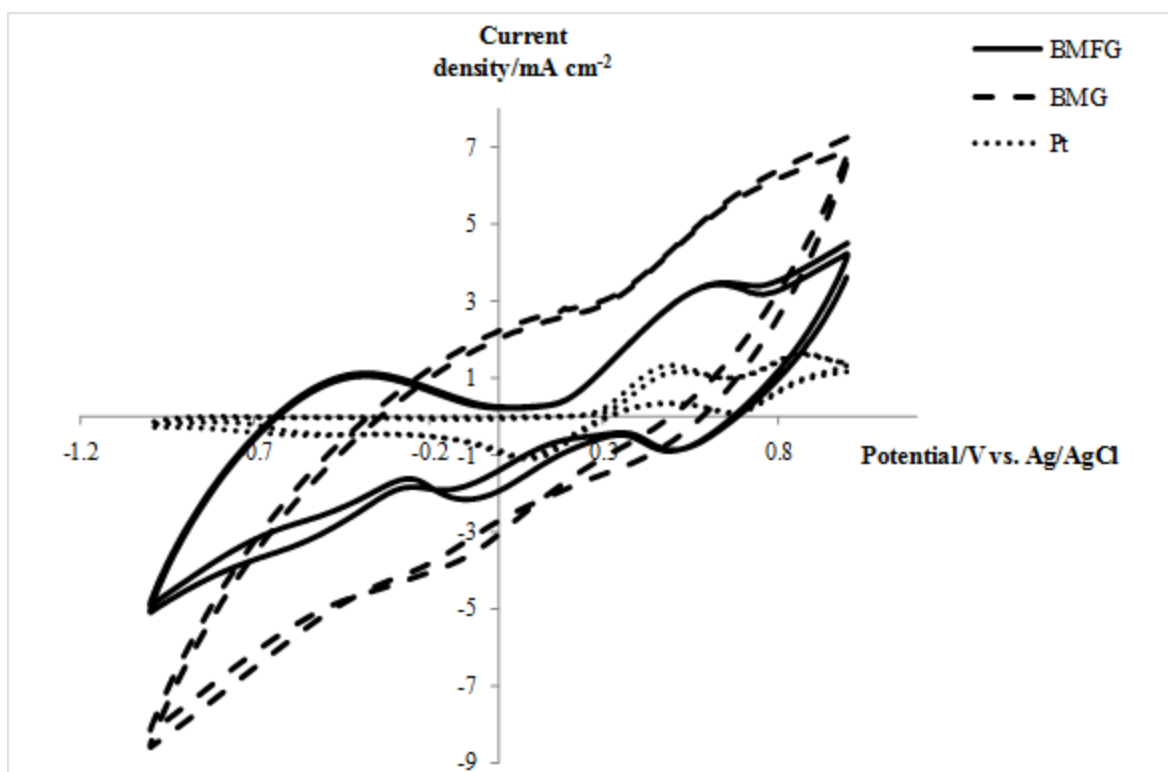(a)   (b)

Fig. 1. (a) Floated graphite layer formed at the surface of water, removal of the floated graphite layer using a glass slide and as-collected graphite (BMFG) on glass and (b) graphite counter electrodes prepared using doctor-blading method.

Figr-2

Fig. 2. Raman spectra of the BMG (upper) and BMFG (lower) samples. The D band appears in BMFG sample due to the edge effects.
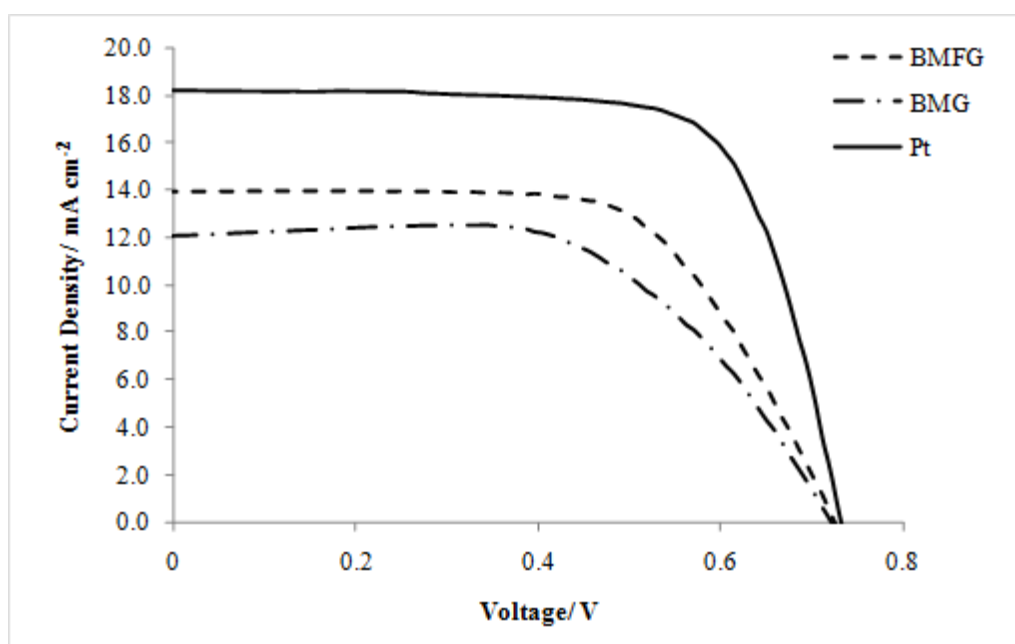
14

Figr-3

Fig. 3.   Cyclic voltamogrammes of electrodes based on BMFG, BMG and Pt/Cr-mirror type, in 10 mM LiI, 1 mM I$_2$, 0.10 M NaClO$_4$ in an acetonitrile electrolyte, at 50 mV s-1 obtained using Ag/AgCl reference electrode and Pt-gauze counter electrode.

15

Figr-4

Fig. 4. J-V characteristics of DSCs employing CEs prepared using BMG, BMFG and Pt CEs.

Table 1. Carbon content of the graphite samples as determined by total carbon analysis.

Carbon Content as Weight%	High	Moderate	Low
BMG	95.9	92.9	91.9
BMFG	98.0	97.3	98.0

Table 2. Photovoltaic parameters of DSCs employing BMFG-based CE prepared with different amounts of morphol.

Mass of morphol added to 0.10 g of graphite/g	Graphite:Morphol mass ratio	J_{SC}/mAcm^{-2}	V_{OC} /V	FF	η/%
0.02	5:1	8.92	0.670	0.22	1.32
0.04	5:2	11.64	0.706	0.55	4.55
0.06	5:3	13.44	0.700	0.58	5.43
0.08	5:4	11.51	0.708	0.44	3.60
0.10	1:1	10.12	0.635	0.36	2.31

Table 3. Photovoltaic parameters of DSCs employing graphite CEs sintered at different temperatures.

Temperature/ °C	J_{SC} /mA cm^{-2}	V_{OC} /V	FF	η/%
250	10.24	0.653	0. 34	2.29
300	13.21	0.717	0.54	5.10
350	13.47	0.704	0.60	5. 67
400	12.82	0.700	0.49	4.43

Table 4. Photovoltaic parameters of DSCs employing CEs with different thicknesses of the graphite layer

Thickness/μm	J_{SC} /mA cm^{-2}	V_{OC} /V	FF	η/%
160	12.94	0.714	0.64	5.94
250	13.89	0.725	0.64	6.47
330	13.57	0.716	0.59	5. 78
460	12.37	0.701	0.53	4.56
550	9.93	0.703	0.48	3.35

Table 5. Photovoltaic parameters of DSCs employing CEs with different compositions

Counter electrode	J_{SC} /mA cm^{-2}	V_{OC} /V	FF	η/%
FTO/Graphite-BMFG	13.89	0.725	0.64	6.47
FTO/Graphite-BMG	12.04	0.726	0.60	5.21
FTO/Pt-Cr	18.18	0.732	0.721	9.60